AD-A054 272 SPERRY RESEARCH CENTER SUDBURY MASS F/G 20/12
MAGNETIC LPE CRYSTALLINE FILMS FOR SMALL-BUBBLE-DIAMETER CYLIND--ETC(U)
OCT 77 M KESTIGIAN, W R BEKEBREDE, A B SMITH F44620-76-C-0121
UNCLASSIFIED SCRC-CR-78-9 AFAL-TR-77-257 NL

| OF |
AD A054272

END
DATE FILMED
6 -78
DDC

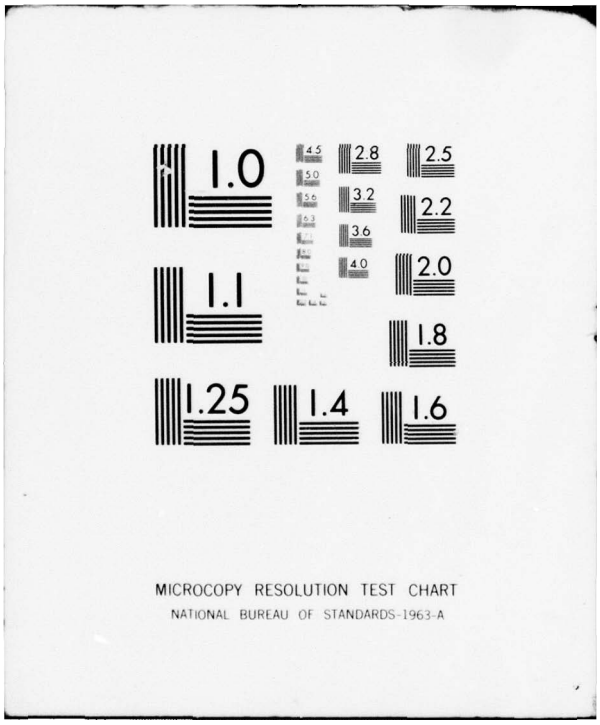
1.0
1.1
1.25
1.4
1.6
1.8
2.0
2.2
2.5
2.8
3.2
3.6
4.0
4.5
5.0
5.6
6.3
MICROCOPY RESOLUTION TEST CHART
NATIONAL BUREAU OF STANDARDS-1963-A

AFAL-TR-77-257

MAGNETIC LPE CRYSTALLINE FILMS FOR SMALL BUBBLE DIAMETER CYLINDRICAL-DOMAIN MEMORY APPLICATIONS

M. Kestigian, W. R. Bekebrede and A. B. Smith

Sperry Research Center
100 North Road
Sudbury, Massachusetts 01776

October 1977
Technical Report AFAL-TR-77-257
Final Report for Period 15 May 1976 to 30 September 1977

AIR FORCE AVIONICS LABORATORY
AIR FORCE WRIGHT AERONAUTICAL LABORATORIES
AIR FORCE SYSTEMS COMMAND
WRIGHT-PATTERSON AIR FORCE BASE, OHIO 45433

NOTICE

When Government drawings, specifications, or other data are used for any purpose other than in connection with a definitely related Government procurement operation, the United States Government thereby incurs no responsibility nor any obligation whatsoever; and the fact that the government may have formulated, furnished, or in any way supplied the said drawings, specifications, or other data, is not to be regarded by implication or otherwise as in any manner licensing the holder or any other person or corporation, or conveying any rights or permission to manufacture, use, or sell any patented invention that may in any way be related thereto.

This report has been reviewed by the Information Office (OI) and is releasable to the National Technical Information Service (NTIS). At NTIS, it will be available to the general public, including foreign nations.

This technical report has been reviewed and is approved for publication.

Dr. Millard G. Mier

FOR THE COMMANDER

Robert D Larson

"If your address has changed, if you wish to be removed from our mailing list, or if the addressee is no longer employed by your organization please notify AFAL/DHR *, W-PAFB, OH 45433 to help us maintain a current mailing list".*

Copies of this report should not be returned unless return is required by security considerations, contractual obligations, or notice on a specific document.

UNCLASSIFIED

SECURITY CLASSIFICATION OF THIS PAGE (When Data Entered)

REPORT DOCUMENTATION PAGE

READ INSTRUCTIONS BEFORE COMPLETING FORM

1. REPORT NUMBER: AFAL-TR-77-257	2. GOVT ACCESSION NO.
3. RECIPIENT'S CATALOG NUMBER	
4. TITLE (and Subtitle): MAGNETIC LPE CRYSTALLINE FILMS FOR SMALL-BUBBLE-DIAMETER CYLINDRICAL-DOMAIN MEMORY APPLICATIONS.	5. TYPE OF REPORT & PERIOD COVERED: Final Report. 15 May 1976 – 30 Sep 1977
	6. PERFORMING ORG. REPORT NUMBER: SCRC-CR-78-9
7. AUTHOR(s): M. Kestigian, W. R. Bekebrede, A. B. Smith	8. CONTRACT OR GRANT NUMBER(s): F44620-76-C-0121
9. PERFORMING ORGANIZATION NAME AND ADDRESS: Sperry Research Center, 100 North Road, Sudbury, MA 01776	10. PROGRAM ELEMENT, PROJECT, TASK AREA & WORK UNIT NUMBERS
11. CONTROLLING OFFICE NAME AND ADDRESS: Air Force Avionics Laboratory, Air Force Wright Aeronautical Laboratories, Air Force Systems Command, Wright Patterson AFB, Ohio 45433	12. REPORT DATE: Oct 1977 13. NUMBER OF PAGES: 47
14. MONITORING AGENCY NAME & ADDRESS (if different from Controlling Office)	15. SECURITY CLASS. (of this report): Unclassified 15a. DECLASSIFICATION/DOWNGRADING SCHEDULE

16. DISTRIBUTION STATEMENT (of this Report)

Approved for public release; distribution unlimited.

17. DISTRIBUTION STATEMENT (of the abstract entered in Block 20, if different from Report)

18. SUPPLEMENTARY NOTES

19. KEY WORDS (Continue on reverse side if necessary and identify by block number)

Small bubble diameter	Temperature dependence
Crystalline garnet films	Stability factor
Liquid-phase epitaxy	Stripe width
Bubble memory devices	Bubble collapse field
Mobility	

micrometers

20. ABSTRACT (Continue on reverse side if necessary and identify by block number)

The objective of the research was to develop a small-bubble-diameter garnet-crystalline magnetic film with useful device properties. Rare-earth iron garnet crystalline compositions were formulated, films deposited by liquid-phase epitaxy, and magnetic evaluation measurements performed. The results of the magnetic property experiments were used to select improved rare-earth iron garnet compositions and film deposition parameters for 2 μm or less bubble-diameter magnetic memory applications. Representative results of over 600 LPE film preparations and delivered samples are given in tabular form. Of the materials investigated, samarium thulium-, yttrium samarium thulium-, yttrium samarium lutetium-, and yttrium europium thulium gallium iron garnet were found to possess static bubble

(Continued on reverse side)

next Page

DD FORM 1 JAN 73 1473 EDITION OF 1 NOV 65 IS OBSOLETE

UNCLASSIFIED

SECURITY CLASSIFICATION OF THIS PAGE (When Data Entered)

408 199

20. ABSTRACT

properties suitable for small bubble diameter applications. Yttrium samarium lutetium calcium germanium iron garnet small-bubble-diameter films were prepared and evaluated for comparison of their magnetic properties. In addition to the static magnetic property experiments, dynamic measurements were performed on $(LaEuTm)_3(FeGa)_5O_{12}$, $(SmTm)_3(FeGa)_5O_{12}$, $(YSmLuCa)_3(FeGe)_5O_{12}$ and $(YSmTm)_3(FeGa)_5O_{12}$. Mobilities of 233, 140, 1000 and 660 cm/sec/Oe, respectively, were determined for representative samples. It was concluded that these materials will be useful for small-bubble-diameter cylindrical-domain memory-device applications.

FOREWORD

This final technical report covers the research performed under Contract No. F44620-76-C-0121 from 15 May 1976 to 30 September 1977.

The contract was with the Electronic Materials Department of the Applied Physics Laboratory, Sperry Research Center, Sudbury, Massachusetts 01776 for Magnetic LPE Crystalline Films for Small-Bubble-Diameter Cylindrical-Domain Memory Applications, and was conducted under the direction of Dr. Millard Mier, AFAL/DHE, Avionics Laboratory, Wright-Patterson Air Force Base, Ohio.

W. R. Bekebrede, M. Kestigian and A. B. Smith were involved in the program and in the preparation of this report. The authors wish to acknowledge the contributions of F. A. Bradlee, F. G. Garabedian and W. Goller.

TABLE OF CONTENTS

LIST OF ILLUSTRATIONS

LIST OF TABLES

SECTION I

INTRODUCTION

1. CONTRACT OBJECTIVE

This research is concerned with the preparation, characterization and evaluation of crystalline garnet magnetic films. The liquid-phase epitaxial growth technique was used to deposit magnetic thin films on commercial non-magnetic 3G substrates. These thin films were evaluated for use in small-bubble-diameter cylindrical-domain memory devices. Research performed in addition to formulation and thin film deposition studies included measurement of wall energy, anisotropy, temperature coefficient, temperature range and magnetization. Analyses involved the presence of impurities, nonstoichiometry and charge compensation considerations. The goal is to prepare and evaluate a small-bubble-diameter (less than 2 μm) LPE crystalline garnet film with the following characteristics:

wall energy density = 0.25 ergs/cm^2

$q = H_k/4\pi M_s > 3$

velocity > 1000 cm/sec @ ΔH = 5 Oe

temperature coefficient = 0.2%/°C

rotating field drive at 10^6 bit/sec shift rate < 25 Oe

2. BACKGROUND

The overall technical approach to be used in the development of a small-bubble-diameter cylindrical-domain mass-memory material emphasizes the formulation, preparation, characterization, evaluation and testing of magnetic crystalline thin films.

The rare-earth iron-garnet magnetic thin films have been found to be the most promising 3 to 8 μm-bubble-diameter materials for bubble memory devices. Large cross sectional area films of suitable perfection and desirable magnetic properties have been obtained from liquid-phase epitaxial deposition experiments. It is reasonable to assume that these successes can be extended to include small-bubble-diameter garnet compositions.

Gadolinium gallium garnet (3G) has found widespread use as the non-magnetic substrate material for the LPE deposition of magnetic garnet thin films. No doubt research extended to include 1 and 2 μm-bubble-diameter materials will also utilize 3G substrates. Since polished 3G substrate slices of adequate quality are readily available commercially, gadolinium gallium garnet boules will not be grown. However, if for any reason commercial substrate sources are not adequate for the deposition of small-bubble-diameter thin films, nonmagnetic garnet single crystals will be grown from the direct melt by the Czochralski technique, oriented crystallographically, cut, polished and cleaned prior to use.

The approach to be followed in the growth of magnetic crystalline films will be the liquid-phase epitaxial method. This technique has proven to be the superior method for obtaining high perfection magnetic films. While both tipping and dipping modifications of LPE growth have been employed, the horizontal wafer-dipping reverse-rotation process will be used for the growth of small-bubble-diameter crystalline thin films.

The selection of the optimum small-bubble-diameter crystalline garnet composition will take into consideration the results of several fundamental magnetic property measurements. Dynamic conversion, hard bubble suppression, propagation angle, mobility, coercivity, temperature dependence of magnetic properties and anisotropy are parameters that must be investigated and understood. These experiments must be supplemented by magnetization, bubble diameter and bubble collapse measurements on all samples.

Compositions to be grown and evaluated include samarium thulium-yttrium samarium lutetium- and europium thulium iron-garnet (all of which contain gallium as the non-magnetic cation diluent) and yttrium samarium lutetium calcium- and yttrium europium lutetium calcium-iron garnet (which contain germanium as the nonmagnetic cation). Investigations will be conducted with the objective of preparing a rare earth iron garnet composition which concentrates all of the transition metal nonmagnetic cations exclusively in the tetrahedral site. The use of germanium instead of gallium approaches this condition. Another approach that might prove to be superior would be to use vanadium, together with a monovalent cation for charge compensation.

SECTION II

EXPERIMENTAL

1. SUBSTRATES

a. Substrate Procurement

Gadolinium gallium garnet (3G) substrates have been obtained as polished wafers from Allied Chemical Company. The specifications under which these wafers were purchased are as follows:

Diameter = 1 inch

Thickness = 0.020 inch

Flat to 3 fringes over central 85% of area

Core, birefringence, and inclusion free

Crystallographically oriented to within 0.5 degrees of [111].

Five or fewer defects over central 85% of area, as revealed by a 2-minute etch in 220° C phosphoric acid, using Nomarski interference contrast microscope.

b. Substrate Processing

Each 3G wafer, immediately prior to being used as an epitaxial substrate, is cleaned by the following sequence of steps:

1) Rinse in acetone
2) Rinse in demineralized water
3) Boil in trichloroethylene for $\frac{1}{2}$ hour
4) Boil in 10% sodium hydroxide for $\frac{1}{2}$ hour
5) Rinse in demineralized water
6) Immerse in phosphoric acid at 120°C for 1 minute
7) Rinse in hot tap water
8) Rinse in demineralized water
9) Blow dry with filtered air gun

Substrate surface quality is a prime requisite for the growth of defect-free bubble-domain epitaxial garnet thin films. The above procedures have produced substrate surfaces of sufficient quality to meet this requirement. It is mentioned that meticulous care must be exercised to maintain the

surface quality of the substrate material until all of the deposition and processing steps have been completed.

2. LIQUID-PHASE EPITAXIAL GARNET FILM GROWTH

The basic liquid-phase epitaxy (LPE) growth procedure used throughout this contract period is conventional for bubble memory films and utilizes horizontal dipping of [111] crystallographically oriented $Gd_3Ga_5O_{12}$ (3G) polished substrates.

The substrate is cleaned prior to use and is supported by a three-pronged platinum wire holder. A lowering-rotation mechanism is used to position the substrate above the solution for pre-heat purposes until temperature equilibrium is reached. Excessive exposure to the vapors above the solution causes defects to form, whereas insufficient heating results in uncontrolled film deposition. The growth process must be carried out under isothermal conditions. Any temperature fluctuations during the growth process produce pronounced film property differences.

Kanthal wound-electrically heated-resistance furnaces were used in the LPE experiments. The temperature profile in a single zone furnace is determined largely by furnace geometry, conduction losses from the furnace ends and by the position of baffles which minimize convection currents. A zone uniform in temperature $\pm$ 1° was 8 cm in length and decreased by 2° one-half inch above the solution surface.

Garnet films were grown on [111] 3G substrates by LPE techniques previously described by numerous researchers. During this study, the substrates were rotated-reverse rotated with a 2-second period at a rate of 60 rpm. Rotation rates less than 30 rpm and greater than 100 rpm led to a degradation of thickness uniformity. A 600 rpm rotation was used when the grown film was withdrawn from the solution. This procedure resulted in obtaining higher quality magnetic films, as any flux residue that had adhered to the film was removed quickly by this procedure.

Succeeding LPE film growth experiments were carried out after immediate magnetic property measurements were performed. These characterization studies included lattice-match-mismatch, film thickness, bubble diameter, magnetization, ℓ , q and anisotropy measurements. Adjustment in solution

composition, deposition procedure and deposition conditions were made on the basis of these evaluation measurements. We realize these evaluation studies do not include dynamic properties; however, unless a film composition exhibits the desired static magnetic properties, it will not meet contract objectives. What this preliminary evaluation procedure does accomplish is that sufficient results are obtained to direct succeeding film growth studies with a minimum of lapsed time.

Saturation temperature T_S was defined for each solution as the temperature at which the growth rate was just discernible (less than 0.05 μm/min for a minimum growth time of 10 minutes). Film deposition was carried out 10 to 20° below the observed saturation temperature for any given solution.

Distribution coefficients employed during this phase of the program were controlled such that the garnet phase was the stable species in any growth process, regardless of film deposition or solution composition modifications. A listing of all R values and/or adjustments would serve no meaningful purpose and is omitted to conserve space and to yield a simpler, more manageable report.

During the course of this contract, over 600 LPE film depositions have been made in the search for an improved small-bubble-diameter crystalline composition. A typical melt composition for the LPE growth of $(YSmTm)_3(GaFe)_5O_{12}$ garnet films in mole per cent is as follows:

Y_2O_3	0.149
Sm_2O_3	0.057
Tm_2O_3	0.028
Ga_2O_3	0.544
Fe_2O_3	8.915
PbO	85.187
B_2O_3	5.120

This preparation yields films with less than two micrometer bubble diameter at a growth rate of approximately 1.0 μm/minute.

3. MAGNETIC FILM CHARACTERIZATION

a. Introduction and Methods

The magnetic characterization of a bubble material involves the measurement of a variety of parameters. Perhaps the most fundamental of these measurements is the determination of magnetization, $4\pi M$, and wall energy σ_w, since all the static bubble properties can be deduced from these two parameters. Alternatively, one can express the static bubble properties in terms of $4\pi M$ and the characteristic length ℓ, which is related to σ_w and $4\pi M$ according to the familiar relationship

$$\ell = \frac{\sigma_w}{4\pi M^2}$$

To determine these basic parameters, we use the Fowlis-Copeland technique[1,2] in which one measures the stripe width and bubble collapse field. The $4\pi M$, σ_w, and ℓ can readily be calculated from these results using the formulas given in references 1 and 2.

As with room-temperature measurements, the temperature dependence of $4\pi M$ and ℓ can also be obtained using the Fowlis-Copeland technique. In obtaining the results presented below, the sample temperature was controlled with a specially constructed hot stage in which a controlled flow of nitrogen gas was used to obtain both hot and cold temperatures. The gas was heated by an electric heater or cooled by passing through a copper tube immersed in liquid nitrogen. No heater was incorporated in the sample chamber itself because such heaters (unless very specially wound) generate magnetic fields that would interfere with the measurement. The sample chamber was designed so that the hot (or cold) gas does not pass directly over the sample; instead, it heats (or cools) the closed chamber in which the sample resides. This arrangement insures that the sample temperature is the same as that of the metal sample chamber which can readily be monitored with a thermocouple. Small, thin glass windows above and below the sample permit light to pass through the sample chamber so that the required observations of the domains can be made using a polarizing microscope which is conventional except for the addition of a special television monitoring system, which is described below.

Several precautions are necessary to avoid an appreciable amount of scatter in the stripe width measurements. This scatter will occur unless the stripe domains are relatively straight over a distance that is at least ten times their width. However, this is not the configuration that the domains normally adopt after the application of either a dc or an ac field perpendicular to the sample. To obtain the desired long, straight domains, we apply an in-plane ac field[2]. We also rotate the sample to find the orientation which gives the straightest stripes. This procedure is required because the stripes have obvious preferred directions reflecting the symmetry in the [111] plane of the sample. A relatively large in-plane field is required for this initial straightening procedure; then before each measurement, a smaller field is used which is just sufficient to cause a noticeable vibration of the domain walls. This motion insures that the coercivity is overcome so that the domains can assume their equilibrium width at each new temperature. The in-plane field is generated by passing up to $\sim$ 5A at 60 Hz through a pair of 100-turn rectangular Helmholtz coils having inside dimensions of $\sim$ 4 x 14 cm.

In order to obtain bubble collapse field data, it is necessary to generate new bubbles at each measuring temperature. To avoid the necessity for opening the stage to cut stripes into bubbles, we have installed a small coil just outside the sample chamber. This is a two-layer pancake coil wound with 15 turns of No. 30 wire on a 6.5 mm o.d. nylon form 0.9 mm thick. Using a pulse generator of 10A maximum output and 0.015 μ-sec rise time, a combination of pulse width and bias field which will cut stripes into bubbles is determined experimentally for each new sample. It is true that these pulses may generate some hard bubbles. However, in experiments on these and many other materials, we have found that some normal bubbles are <u>always</u> generated also. Our results are not affected by the hard bubbles, since we read the collapse field of the <u>first</u> isolated bubble to collapse and this must be one of the normal bubbles.

In addition to measurements of ℓ and $4\pi M$, we have also made room-temperature measurements of the anisotropy constant K_u. This is one of the most important bubble material parameters, since it determines bubble stability and influence ℓ according to the relation

$$\ell = \frac{\sqrt{AK_u}}{\pi M^2} \qquad (1)$$

(where A is the exchange constant). In our measurements of K_u, we have used the Kurtzig-Hagedorn method[3,4,5] in which one observes the magnitude of in-plane field required to extinguish the stripe domains observed via the Faraday effect. The details of the experimental procedure for making this measurement may be found in reference 4. The magnitude of K_u is determined from these experiments by using the method described by Druyvesteyn et al[6].

An important auxiliary parameter that can be calculated from the basic material parameters is the bubble stability factor q. This parameter is the ratio between the anisotropy field and the magnetization. Since the anisotropy field is equal to $2K_u/M$, the q is given by

$$q = \frac{K_u}{2\pi M^2} \qquad (2)$$

Because of the importance of this parameter to bubble device applications, we will frequently give this parameter in addition to K_u, ℓ, and $4\pi M$.

b. Magnetic Film Processing Procedures

The as-grown LPE film is immediately cleaned in nitric acid to remove any excess flux which has adhered to it upon withdrawal from the melt. It is then rinsed in demineralized water and blown dry, after which it is ready for characterization.

The film is first examined for the presence of defects on a Leitz metallurgical microscope equipped with Nomarski interference contrast. In general, defects arise in two ways: 1) by propagation from the surface of the substrate, and 2) by incorporation during growth from precipitates or other foreign bodies in the melt. Good quality, clean, properly handled substrates essentially eliminate the propagated variety. The others are controlled by careful preparation of the melt and proper temperature control to insure that precipitation does not occur.

c. Film Thickness Measurements

Epitaxial film thicknesses were measured by optical interference on a Leitz metallograph fitted with a Bausch & Lomb grating monochrometer. The film thickness at any point on the wafer can be calculated by measuring the wavelength change required to cause the fringe system to move an integral number of fringe widths. In addition, the static fringe pattern, i.e., at a fixed wavelength, shows at a glance how uniform the film thickness is. The LPE films delivered under the subject contract have been flat to within one fringe (about 0.1 μm) over the central 85% of the area. There are unavoidable thickness variations in the immediate vicinity of the contact points where the substrate is held in its platinum holder during film growth.

d. Film-Substrate Lattice Parameter Measurements

The relative lattice parameter of the LPE film, i.e., how well it matches that of the substrate, is measured by x-ray diffraction, using a Philips wide-angle goniometer and copper $K\alpha$ radiation. The film and substrate (888) reflections are recorded and their angular difference is a measure of Δa, the film/substrate mismatch. Precision is enhanced by the use of a very narrow ($1/12^{\circ}$) divergence slit and the smallest goniometer speed ($1/8^{\circ}$/minute). The lowest value of Δa measurable by this technique is about 0.005Å, below which the film and substrate reflections are not resolved. All films delivered thus far had Δa values < 0.005Å.

e. Static-Film Property Measurements

Before presenting the results of our measurements of small-bubble garnets, a brief introduction is necessary to put these results in perspective. A general formula for the bubble garnet materials we have grown is:

$$(R' R'' R \ldots.)_3 Fe_{5-x} N_x O_{12}$$

where: R_1, R_2, etc. are rare earths (or yttrium or calcium)

N is a non-magnetic ion, such as Ga or Ge.

The fundamental properties of a garnet, such as the uniaxial anisotropy constant and the inherent damping of the wall motion, are determined almost entirely by the rare earths (R', R'', etc.) in the above formula. We will

therefore identify compositions primarily by the rare earths they contain. We will consider that all films with the same rare earth content are basically the same composition, even if x is not the same in all samples. This is not to say that x has no effect on some important bubble properties. The $4\pi M$ depends directly on x and changes[7] by about 150.G for a change of 0.1 in x. Therefore, variations in x will change both ℓ and q, since these quantities depend on $4\pi M$. Since K_u and A do not vary appreciably for modest changes in $4\pi M$, ℓ and q vary predictably with $4\pi M$ according to the relation

$$\ell \propto q \propto \frac{1}{M^2} \tag{3}$$

which follows directly from Eqs. (1) and (2).

In practice, LPE garnets are prepared by growing test films and making small additions to the melt until x has the value which gives a desired bubble diameter. By making such melt additions, we have grown a series of films with a range of different bubble diameters for each basic composition that we chose to study. To present here the data on all these samples of each R', R''.... combination would take a great deal of space and would merely serve to obscure rather than clarify the significant conclusions that can be drawn from our experiments. Instead, we present in Table just one set of data for each rare earth combination. Even though we are thus compressing a large amount of experimental data into a relatively few numbers, we still retain (as will be demonstrated below) all the essential information on the static bubble properties of each composition. Thus the experimental data on individual samples can be relegated to Appendices A and B without losing any information needed for a general discussion of the relative merits of the different compositions we have prepared.

Except for one composition, the data in Table 1 represents a summary of results on several films. Thus the values shown for K_u indicate the range of values obtained upon measuring several samples. It will be seen that these ranges are relatively small since, as mentioned above, K_u is expected to be the same for all compositions containing the same rare earths R', R''... . Unlike K_u, the parameters $4\pi M$ and q depend directly on x. Therefore,

in order to present the data in a form that can readily be interpreted, it is necessary to separate the dependence on x from differences which are due to the rare earth content R', R''.... . We have chosen to accomplish this by normalizing all data to the same ℓ value. Thus, although we have made measurements on samples with ℓ between 0.1 and 0.7 μm, we have used Eqs. (1) and (2) to calculate what $4\pi M$ and q would have been if ℓ had been 0.15 μm in each sample. Since the average bubble diameter of a material is slightly less than ten times its ℓ value, the values of $4\pi M$ and ℓ presented in Table 1 are therefore the values that would be obtained in a material supporting bubbles of about 1.5 μm diameter. If one wishes to know what $4\pi M$ would correspond to some different ℓ, the value can easily be calculated from the simple relation

$$4\pi M\Big|_{\ell} = \left[4\pi M\Big|_{\ell\,=\,0.15}\right]\left(\frac{0.15}{\ell}\right)^{\frac{1}{2}}$$

which follows directly from Eq. (1). Similarly, the value of q in the table is that value which corresponds to $\ell = 0.15$. To obtain the value of q for some ℓ other than 0.15, one has merely to apply the relation

$$q\Big|_{\ell} = \left[q\Big|_{\ell\,=\,0.15}\right]\frac{\ell}{0.15}$$

which follows directly from Eq. (2).

A wide spectrum of materials is represented in Table 1. Included are several new compositions, as well as some 6 μm bubble materials appropriately modified for small-bubble applications. As may be seen from the table, most of these materials do not fulfill the $q \geq 3$ Air Force requirement when the bubble size is ~ 1.5 μm. Those with $q < 3$ include several compositions which have been often mentioned as potential small-bubble materials. Fortunately, however, there are six compositions in this table which can meet the $q \geq 3$ requirement. One of these materials (the $(YEu)_3(FeGa)_5O_{12}$) can be eliminated from consideration because it has a positive magnetostriction coefficient that prevents hard bubble suppression by ion implantation. Table 1 indicates that the remaining five high-q materials have almost ideal room-temperature

static properties.

The temperature dependence of collapse field and stripe width in these five materials* are shown in Figs. 1 through 4. Over the -55°C to +125°C range, the percentage changes (referred to room temperature) of stripe width and collapse field for these three materials are:

Composition	Stripe Width	Collapse Field
$(LaEuTm)_3(FeGa)_5O_{12}$	17.%	13.%
$(SmTm)_3(FeGa)_5O_{12}$	11.%	24.%
$(TbTm)_3(FeGa)_5O_{12}$	102.%	47%
$(YSmTm)_3(FeGa)_5O_{12}$	14.%	55.%

Clearly, the $(TbTm)_3(FeGa)_5O_{12}$ has a poor temperature dependence, but the other three materials are very good. As a matter of fact, it would be hard to conceive of appreciably less variation being achieved in any bubble garnet. Thus, there are three materials, $(SmTm)_3(FeGa)_5O_{12}$, $(YSmTm)_3(FeGa)_5O_{12}$ and $(LaEuTm)_3(FeGa)_5O_{12}$ with almost ideal static bubble properties. Obviously, our next task was to evaluate their dynamic properties. The results of these measurements are described in the next section.

For the purposes of completeness, we have also prepared and evaluated $(YSmLu)_3(FeGa)_5O_{12}$ and $(YSmLuCa)_3(FeGe)_5O_{12}$ as candidate materials for small bubble diameter applications. These results were presented at the Magnetism and Magnetic Materials Conference in Minneapolis and are given in Appendix C of this report.

f. Dynamic Film Property Measurements

Techniques for measuring static bubble parameters were described in the preceding Section (IIe). This section will discuss dynamic film property measurements that were conducted during the contract period. These measurements have been made using the bubble-shift technique originally described by

*Actually, we measured the temperature dependence of only four of these five compositions. Since Table 1 shows $(EuTm)_3(FeGa)_5O_{12}$ and $(LaEuTm)_3(FeGa)_5O_{12}$ to have similar room temperature properties, we have assumed that their temperature dependences will also be similar and have only measured the $(LaEuTm)_3(FeGa)_5O_{12}$.

TABLE 1

BASIC STATIC BUBBLE DATA FOR
VARIOUS SMALL-BUBBLE GARNETS

Composition	$10^4 K_u$ (ergs/cm^3)	for ℓ = 0.15 μm: q	for ℓ = 0.15 μm: $4\pi M$ (G)
$(YLaTm)_3(FeGa)_5O_{12}$ [d]	0.9-2.0	1.4-1.7	370.-590.
$(YEuLuCa)_3(FeGe)_5O_{12}$ [O,d]	0.4-2.6	0.5-1.7	290.-810.
$(YSmLuCa)_3(FeGe)_5O_{12}$ [d]	0.5-1.1	1.2-1.7	380.-480.
$(YEu)_3(FeGa)_5O_{12}$ [a]	2.5-5.9	1.6-5.1	540.-620.
$(EuTm)_3(FeGa)_5O_{12}$ [b]	6.7	3.9	655.
$(LaEuTm)_3(FeGa)_5O_{12}$ [d]	5.2-7.5	2.9-5.3	520.-790.
$(SmTm)_3(FeGa)_5O_{12}$	12.2	3.9-6.9	670.-880.
$(TbTm)_3(FeGa)_5O_{12}$	9.7-13.0	3.4-5.7	650.-970.
$(LaTm)_3(FeGa)_5O_{12}$	0.8	0.7-1.8	330.-540.
$(YSmTm)_3(FeGa)_5O_{12}$ [d]	1.8-8.7	1.6-4.0	530.-740.

a. This composition was grown on a (110) $Sm_3Ga_5O_{12}$ substrate and was mismatched to this substrate so that the anisotropy was primarily strain induced. All other samples were grown on [111] $Gd_3Ga_5O_{12}$ and were closely matched to the substrate (to within .003Å).

b. Only one sample was measured of this composition. Several samples were prepared of each of the other materials; in cases where not all samples gave the same results, the range of values is indicated. Representative experimental data from which this table was derived may be found in Appendix A.

c. The wide range of observed values for this material may be due to inhomogeneities such as have been reported[8] in other garnets containing Ca or Ge.

d. In garnet films with only two rare earths, there is a unique concentration of each that will permit the film to match the substrate. However, in materials having three rare earths, there is a range of relative concentrations which yield a match. Therefore, although we believe the results given here are typical, there may be other formulations of these compositions yielding somewhat different results.

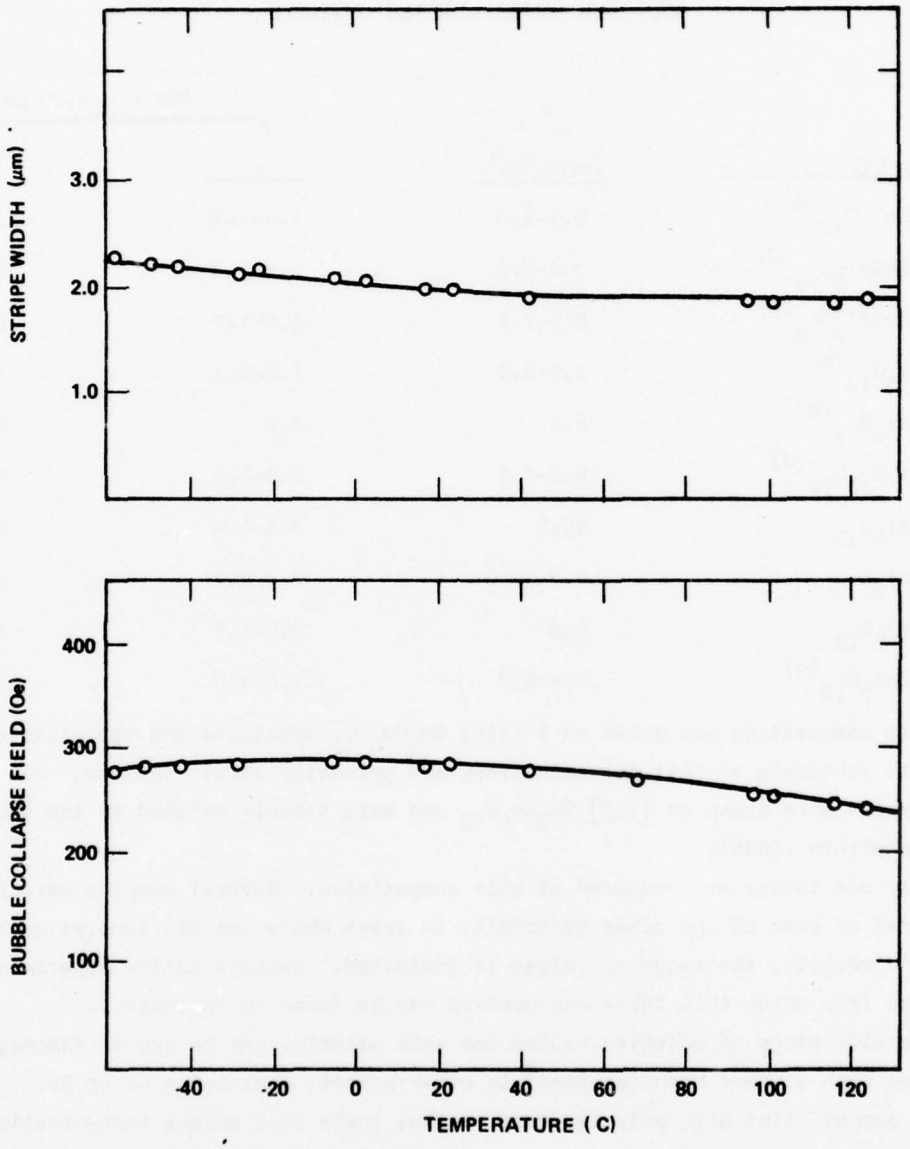

FIG. 1 Stripe width and bubble collapse field for $(LaEuTm)_3(FeGa)_5O_{12}$ as a function of temperature.

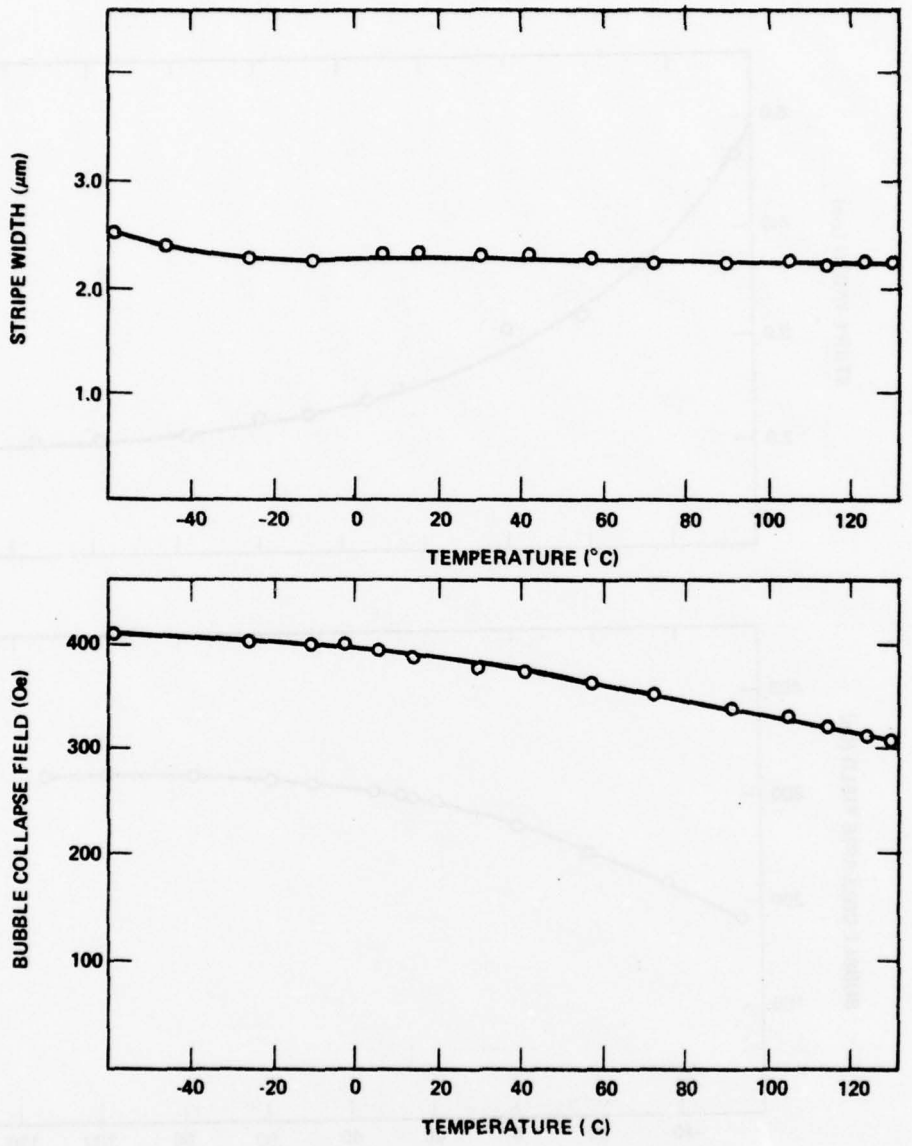

FIG. 2 Stripe width and bubble collapse field for $(SmTm)_3(FeGa)_5O_{12}$ as a function of temperature.

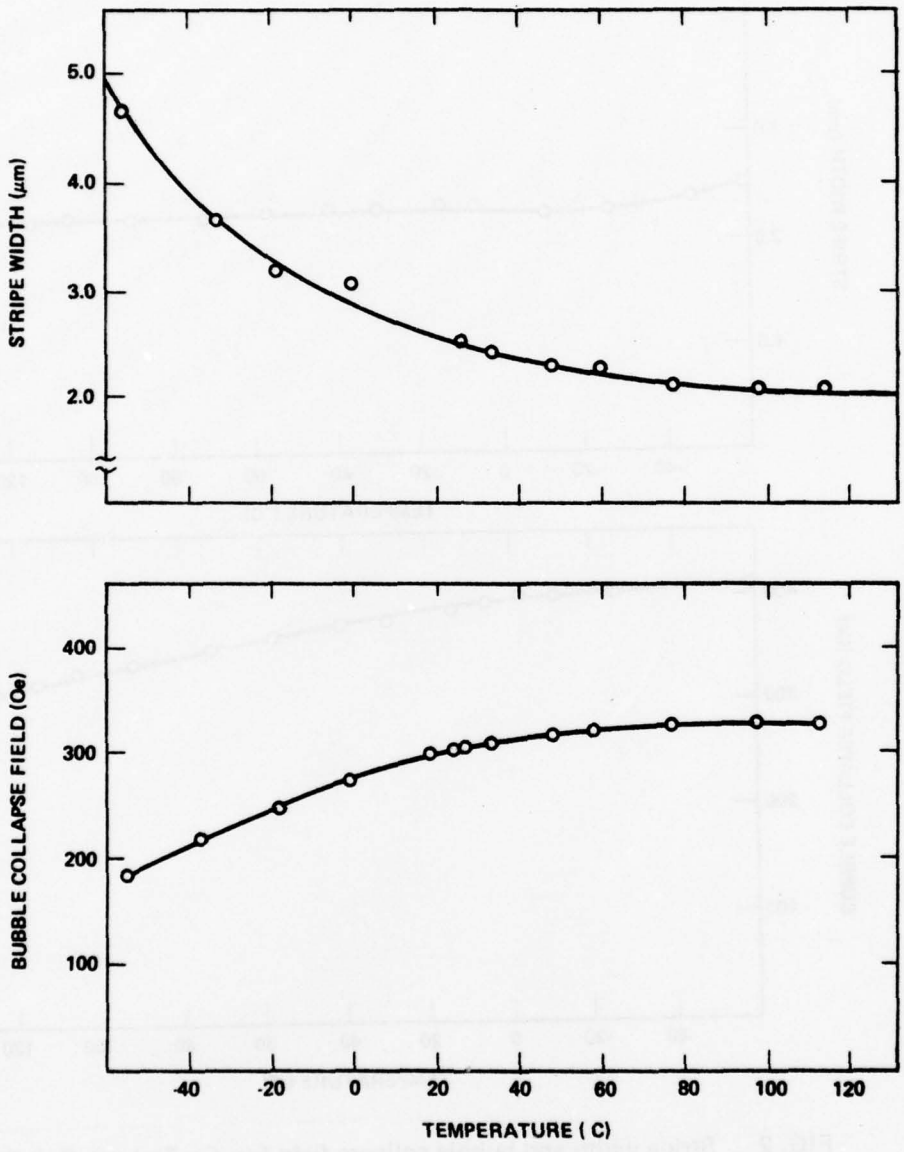

FIG. 3 Stripe width and bubble collapse field for $(TbTm)_3(FeGa)_5O_{12}$ as a function of temperature.

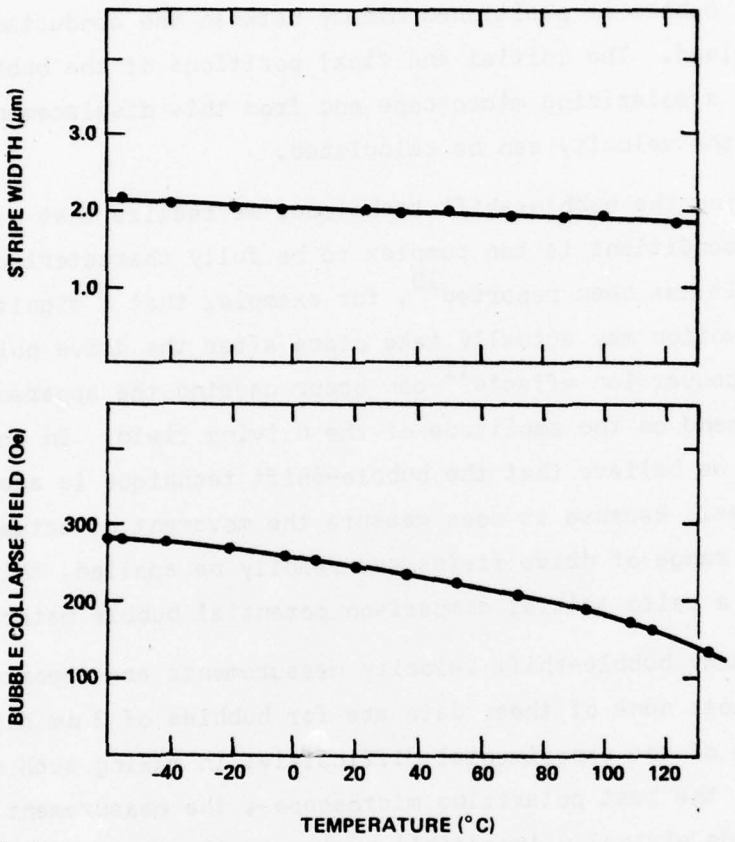

FIG. 4 Stripe width and bubble collapse field for $(YSmTm)_3(FeGa)_5O_{12}$ as a function of temperature.

Vella-Coleiro and Tabor[9]. In this technique, two parallel conductors are placed against the surface of the garnet, as shown in Figure 5. To make the measurement, a bubble is positioned midway between the conductors and the conductors are pulsed. The initial and final positions of the bubble are measured using a polarizing microscope and from this displacement and the pulse length, the velocity can be calculated.

In utilizing the bubble-shift technique, we realize that bubble behavior under dynamic conditions is too complex to be fully characterized by one measurement. It has been reported[10], for example, that a significant amount of the bubble motion may actually take place after the drive pulse has ended. Also, dynamic conversion effects[11] can occur causing the apparent bubble mobility to depend on the amplitude of the driving field. In spite of these complications, we believe that the bubble-shift technique is adequate for our present purposes. Because it does measure the movement of actual bubbles and because a full range of drive fields can readily be applied, this technique should provide a valid initial comparison potential bubble materials.

Although many bubble-shift velocity measurements are reported in the literature, almost none of these data are for bubbles of 3 μm diameter or smaller because of the experimental difficulties in making such measurements. Even when using the best polarizing microscopes, the measurement of bubbles of this size is made virtually impossible by the small dimensions involved and the poor contrast of the image. In order to make such measurements possible, we have purchased a special television system made to our specifications. This system utilizes an ultra-low-light-level camera tube having an integral silicon image intensifier. The output of this tube is then electronically processed to enhance the image by introducing controllable amounts of contrast enhancement, clipping and high-frequency peaking. In addition, a pair of measuring lines is added electronically to the image. The position of these lines is fully adjustable and the distance between them is displayed on a digital meter. A block diagram of this system is shown in Figure 6 and a photograph of the apparatus is shown in Figure 7. We find that this apparatus does allow us to make the small-bubble measurements that previously were either difficult or impossible. Velocity measurements can now be made on bubbles down to 1 μm in diameter. In addition to these dynamic measurements,

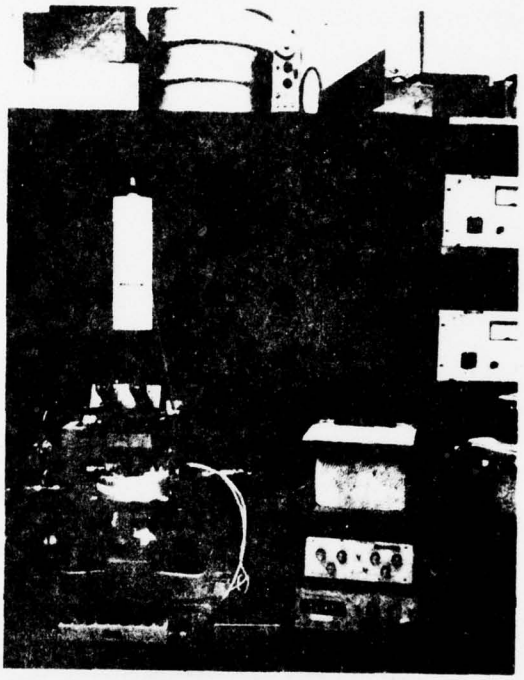

FIG. 7 The microscope and television monitoring system used for the measurement of small bubble materials.

all the static measurements (and particularly the strip width measurements) are made much more conveniently and accurately with the use of the television system.

In Section IIe of this report, we identified three promising materials for small-bubble devices on the basis of their static properties. These materials were $(SmTm)_3(FeGa)_5O_{12}$, $(YSmTm)_3(FeGe)_5O_{12}$ and $(LaEuTm)_3(FeGa)_5O_{12}$. In addition to the room temperature values of all the important bubble parameters, the temperature dependence of stripe width and collapse field for these materials were also given in that section. In order to fully assess the usefulness of these materials for device use, it is also necessary to examine the variation of the anisotropy contant K_u with temperature. If the anisotropy field $H_k = 2K_u/M$ falls below some minimum value, spontaneous nucleation of bubbles can occur in device use. The minimum anisotropy that can be tolerated varies with the circuit type, but one rule of thumb that is frequently used is that the $a = H_k/4\pi M$ should be greater than 3. The results of anisotropy measurements of two of these materials are presented in Figures 8 and 9, where we have plotted the data three different ways, i.e., in terms of K_u, H_k and q.

We see from Figure 8 that the q of $(SmTm)_3(FeGa)_5O_{12}$ is 5.2 at 125°C. Since this sample has an ℓ of 0.16 μm, it would support bubbles with a diameter of approximately 1.6 μm. Since q scales with ℓ, this material could be adjusted to provide 1 μm bubbles with a $q > 3$ at 125°C. This result together with the static property data all indicate that this material is well suited for bubble devices using bubbles as small as 1 μm and covering the entire military temperature range of -55°C to +125°C. Similarly, the data in Figure 9 indicate that $(LaEuTm)_3(GaFe)_5O_{12}$ will provide $q > 3$ for 1.5 μm bubbles and also operate over the full military range.

Having established that the static bubble properties of both $(SmTm)_3(FeGa)_5O_{12}$ and $(LaEuTm)_3(FeGa)_5O_{12}$ are favorable for small bubble applications, we must also determine whether their dynamic behavior is acceptable. Therefore, we have measured the bubble-shift velocity v vs. drive field ΔH for both of these materials. The results are shown in Figures 10 and 11, where we have also indicated for each material the mobility determined[9] from the slope of the curve.

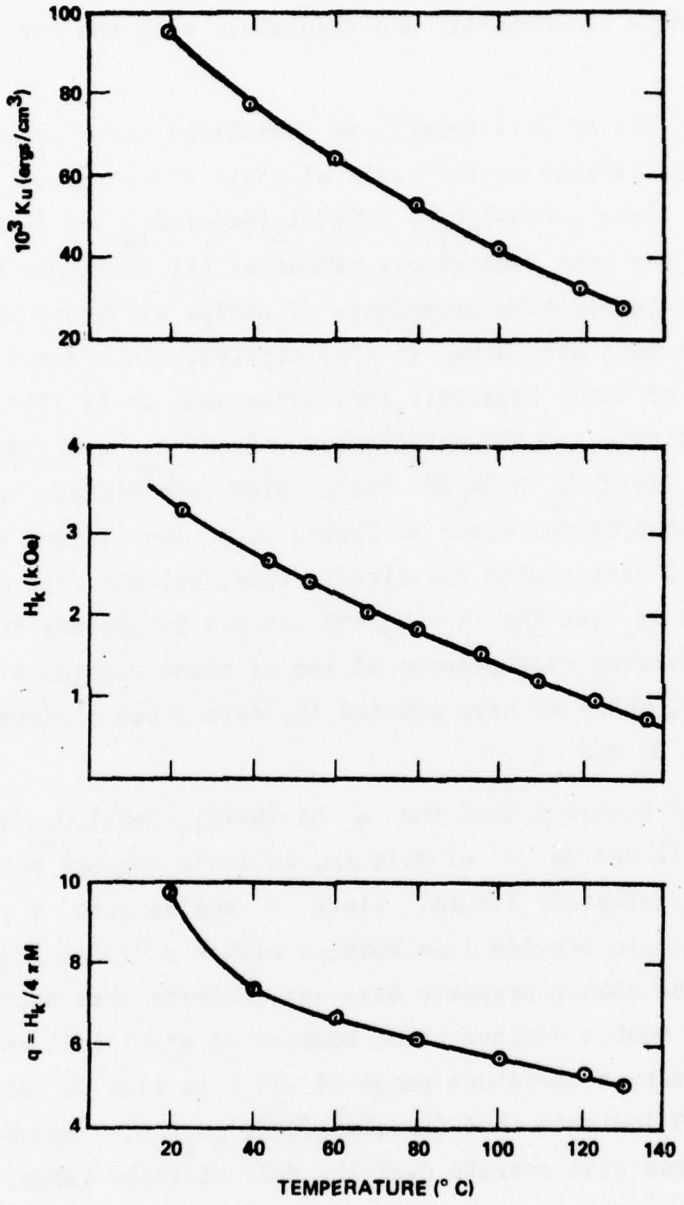

FIG. 8 K_u, H_k and q vs. temperature for a $(SmTm)_3(FeGa)_5O_{12}$ film. (The magnetic parameters of this film at room temperature are: $\ell = 0.16\ \mu m, 4\pi M = 645$ G.)

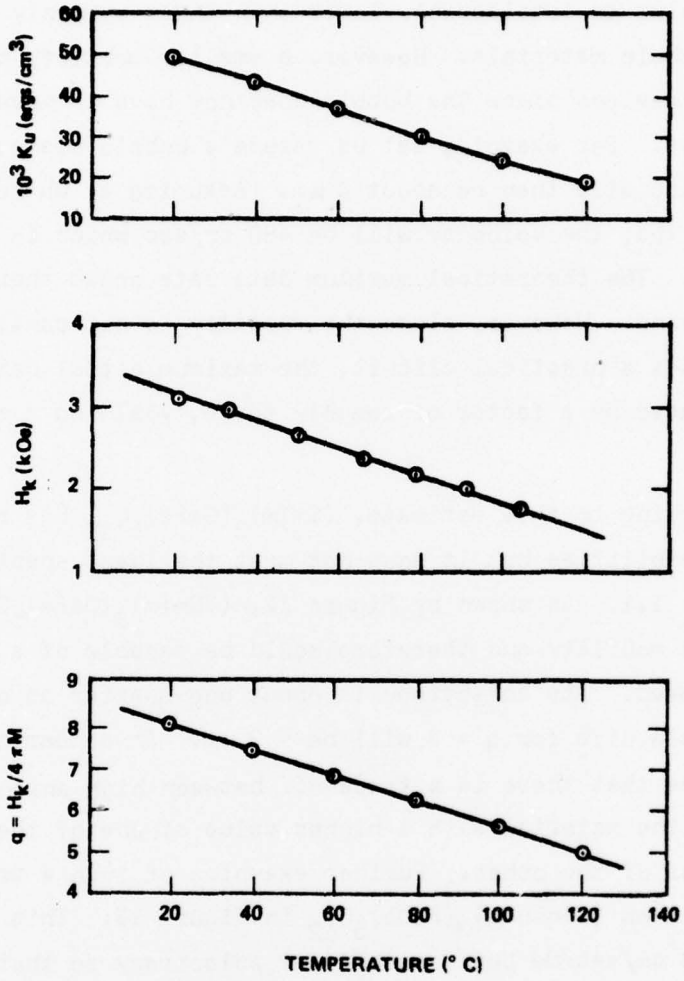

FIG. 9 K_u, H_k and q vs. temperature for $(LaEuTm)_3(FeGa)_5O_{12}$. (The magnetic parameters of this film at room temperature are: ℓ = 0.24 μm, 4 π M = 533 G.)

We see from Figure 10 that $(SmTm)_3(FeGa)_5O_{12}$ has a mobility of 140 cm/sec/Oe. This value is considerably lower than those commonly obtained with 6 μm-diameter bubble materials. However, a smaller mobility can be tolerated in small-bubble devices since the bubble does not have to move as far between circuit positions. For example, let us assume a bubble diameter of 1 μm. The circuit period will then be about 4 μm. Assuming a ΔH of 10 Oe, Figure 10 shows that the velocity will be 480 cm/sec which is 1.2 periods per microsecond. The theoretical maximum data rate would therefore be 1.2 megabits per second. However, since the velocity is not constant as the bubble transverses a practical circuit, the maximum actual data rate would probably be reduced by a factor of roughly three, yielding a rate of ~ 400 k bit/sec.

Thus, according to this estimate, $(SmTm)_3(GaFe)_5O_{12}$ has reasonable device speed capabilities but it does not meet the ideal specifications set forth in Section I.1. As shown by Figure 12, $(YSmTm)_3(GaFe)_5O_{12}$ has a considerably higher mobility and therefore would be capable of a correspondingly higher device speed. Its anisotropy is about one-quarter as big, however, so its minimum bubble size for q = 3 will be ~ 2 μm. In comparing these two materials, we see that there is a trade-off between high anisotropy and high mobility, i.e., the material with a higher value of one of these parameters has a lower value of the other. Further examples of such a trade-off is given by the data on $(YSmLuCa)_3(FeGe)_5O_{12}$ in Figure 13. This material has a mobility of 1000 cm/sec/Oe but a much lower anisotropy so that the minimum bubble size for q = 3 at room temperature is about 3. μm. The ideal bubble material would, of course, have both high mobility and high anisotropy. The materials described above represent the best combination of properties for small-bubble applications yet discovered.

4. CONCLUSIONS

Rare-earth garnet crystalline compositions were formulated, films deposited by liquid-phase epitaxy, and magnetic evaluation measurements performed. The results of the magnetic property experiments were used to select improved rare-earth iron garnet compositions and film deposition conditions for small-bubble-diameter magnetic memory applications. Representative results of delivered samples are given in tabular form in Appendix B. During

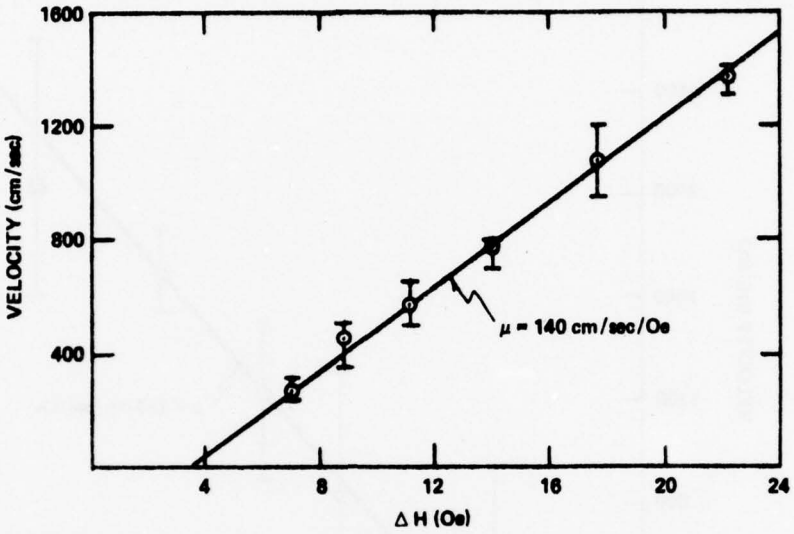

FIG. 10 Velocity vs. drive field for a $(SmTm)_3(FeGa)_5O_{12}$ film having the following properties: thickness = 3.6 μm, ℓ = 0.16 μm, 4 π M = 645 G, H_k = 4657 Oe, $K_u = 1.2 \times 10^5$ erg/cm^3, q = 7.4. (The bars indicate the spread in the data obtained upon repeating each measurement about six times; the circles represent the average of these measurements. The spread indicated by the bars is due primarily to variability in bubble behavior, not to uncertainties in the measurement.)

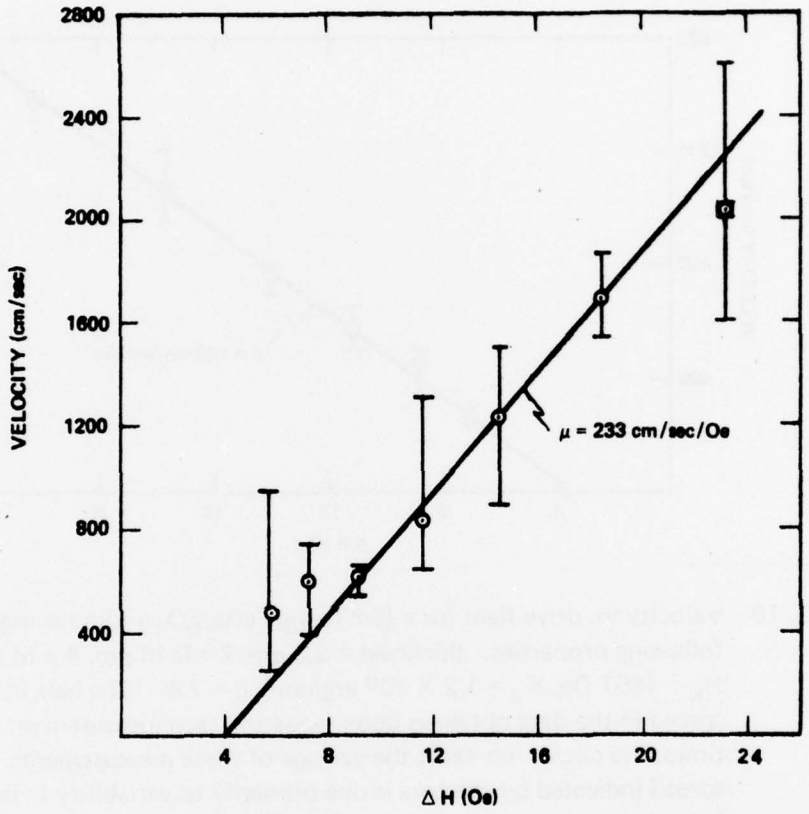

FIG. 11 Velocity vs. drive field for a $(LaEuTm)_3(FeGa)_5O_{12}$ film having the following properties: thickness = 3.6 μm, ℓ = 0.24 μm, 4 π M = 480 G, H_k = 3276 Oe, $K_u = 6.3 \times 10^4$ erg/cm^3, q = 6.9. (The bars indicate the spread in the data obtained upon repeating each measurement about six times; the circles represent the average of these six measurements. The spread indicated by the bars is due primarily to variability in bubble behavior, not to uncertainties in the measurement.)

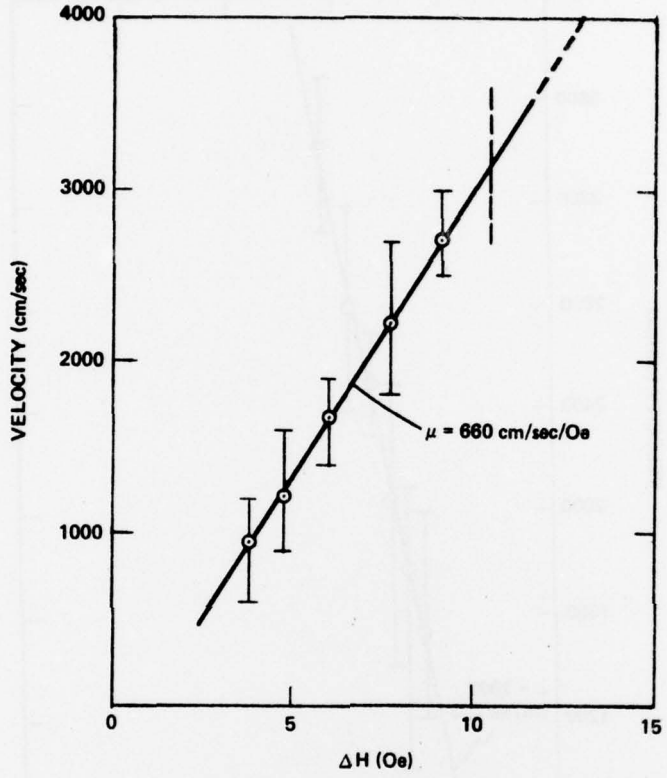

FIG. 12 Velocity vs. drive field for a $(YSmTm)_3(FeGa)_5O_{12}$ film having the following properties: thickness = 2.6 μm, ℓ = 0.19 μm, 4 π M = 400 G, H_k = 1480 Oe, $K_u = 2.37 \times 10^4$ erg/cm^3, q = 3.7. (The bars indicate the spread in the data obtained upon repeating each measurement about six times; the circles represent the average of these six measurements. The spread indicated by the bars is due primarily to variability in bubble behavior, not to uncertainties in the measurement.)

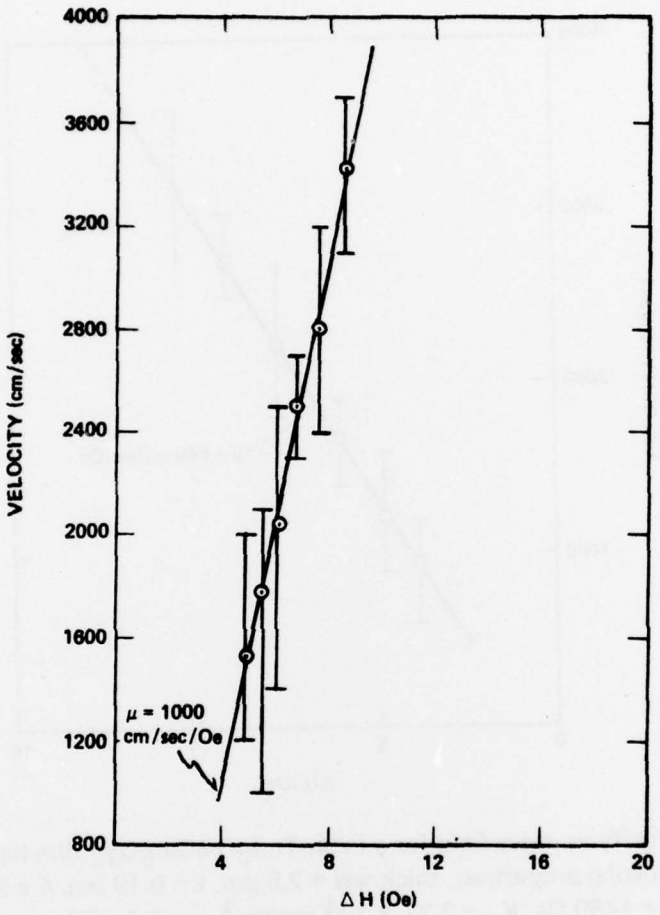

FIG. 13 Velocity vs. drive field for a $(YSmLuCa)_3(FeGa)_5O_{12}$ film having the following properties: thickness = 2.3 μm, 4 π M = 320 G, H_k = 670 Oe, $K_u = 9.7 \times 10^3$ erg/cm^3, q = 2.4. (The bars indicate the spread in the data obtained upon repeating each measurement about six times; the circles represent the average of these six measurements. The spread indicated by the bars is due primarily to variability in bubble behavior, not to uncertainties in the measurement.)

this report period, samarium thulium-, yttrium samarium thulium-,yttrium samarium lutetium-, and yttrium europium thulium gallium iron garnet films were grown and their static magnetic properties evaluated. Yttrium samarium lutetium calcium germanium iron garnet small-bubble-diameter films were prepared and evaluated for comparison of their magnetic properties. In addition to the static magnetic property experiments, dynamic measurements were performed on $(LaEuTm)_3(FeGa)_5O_{12}$, $(SmTm)_3(FeGa)_5O_{12}$, $(YSmLuCa)_2(FeGe)_5O_{12}$ and $(YSmTm)_3(FeGa)_5O_{12}$ films. Mobilities of 233, 140, 1000 and 660 cm/sec/Oe, respectively, were determined for representative samples. It is concluded that these materials will be useful for small bubble diameter cylindircal-domain bubble memory device applications. The final selection process must consider the circuit requirements and ultimate design characteristics, which are beyond the scope of this program.

APPENDIX A

TABULATION OF REPRESENTATIVE SMALL-BUBBLE-DIAMETER EXPERIMENTAL RESULTS

In Table 1 we gave a summary of the experimental data taken on a large number of films. The purpose of this appendix is to present (by means of Table 2) a representative sample of the experimental data on which Table 1 was based. These data in Table 2 include film thickness, zero-field stripe width, $4\pi M$, ℓ, K_u and q . The table also contains the normalized q and $4\pi M$ values which are discussed in connection with Table 1.

APPENDIX A

TABLE 2

TABULATION OF REPRESENTATIVE SMALL BUBBLE DIAMETER EXPERIMENTAL RESULTS

MATERIAL	SAMPLE NUMBER	FILM THICKNESS (μM)	ZERO FIELD STRIPE WIDTH (μM)	4πM (G)	ℓ (μM)	$10^{-4}K_u$ (ergs/cm^3)	q	q	4πM (G)
$(YLaTm)_3(FeGe)_5O_{12}$ [4]	50418B	6.4	3.3	350.	0.228	1.21	2.48	1.63	429.
	50417B	6.6	2.5	402.	0.128	0.917	1.43	1.68	371.
	50605B	1.0	1.0	683.	0.113	~1.96	~1.1	~1.5	593.
	50516C	2.0	1.0	693.	0.067	1.20	0.63	~1.41	463.
$(YEuLaCa)_3(FeGe)_5O_{12}$ [3,4]	60329B	4.3	2.2	539.	0.151	2.01	1.75	1.74	541.
	60406B	3.8	2.1	802.	0.154	2.58	1.01	0.98	813.
	60615A	6.0	3.9	194.	0.329	0.394	2.63	1.20	287.
	60616D	3.8	3.0	355.	0.293	0.5	1.0	0.51	496.
$(YSmLuCa)_3(FeGe)_5O_{12}$ [4]	60922C	2.2	2.2	296.	0.248	0.47	2.8	1.70	380.
	60923B	1.7	2.0	376.	0.242	1.10	1.9	1.18	477.
	60923D	2.1	2.0	325.	0.219	0.89	2.1	1.44	392.
$(YEu)_3(FeGa)_5O_{12}$ [1]	41112A	4.43	1.95	559.	0.140	5.93	4.76	5.10	540.
	41105B	3.88	1.48	866.	0.076	2.49	0.83	1.64	617.
$(EuTm)_3(FeGa)_5O_{12}$ [4]	50625A	3.3	3.0	470.	0.291	6.7	7.64	3.94	655.
$(LaEuTm)_3(FeGa)_5O_{12}$ [4]	60707A	1.0	2.2	483.	0.292	5.2	5.6	2.87	674.
	60708B	2.1	2.4	484.	0.298	5.8	6.2	3.12	683.
	60716B	2.5	1.7	526.	0.149	5.9	5.3	5.3	523.
	60715C	1.8	1.9	650.	0.220	7.5	4.5	3.06	788.
$(SmTm)_3(FeGa)_5O_{12}$	61019A	3.6	2.1	645.	0.161	12.2	7.4	6.9	667.
	61019B	3.6	3.4	561.	0.372	12.2	9.7	3.9	883.
$(TbTm)_3(FeGa)_5O_{12}$	61204A	7.8	6.7	304.	0.694	9.7	26.3	5.7	654.
	61204B	3.1	5.5	441.	0.729	13.0	16.4	3.4	972.
$(LaTm)_3(FeGa)_5O_{12}$	61014D	3.5	1.7	633.	0.110	0.86	0.54	0.74	541.
	61027D	5.8	4.7	188.	0.467	0.77	5.5	1.77	332.
$(YSmTm)_3(FeGa)_5O_{12}$	70707C	2.2	2.5	377.	0.298	1.81	3.2	1.61	531.
	70921C	1.6	1.0	1006.	0.082	8.7	2.16	3.95	744.

APPENDIX B

TABULATION OF MAGNETIC DATA FOR SUBSTRATES AND LPE FILMS DELIVERED TO CONTRACT MONITOR

Once a month since the beginning of this contract, we have sent representative garnet films to WPAFB. The purpose of this appendix is to summarize the properties of these films. In Appendix B, we have listed the composition, film thickness, and magnetic properties for all of these films.

APPENDIX B

TABLE 3

TABULATION OF MAGNETIC DATA FOR SUBSTRATES AND LPE FILMS DELIVERED TO CONTRACT MONITOR

DATE OF SHIPMENT to WPAFB	SAMPLE NUMBER	SAMPLE COMPOSITION	FILM THICKNESS (μm)	ZERO-FIELD STRIPE WIDTH (μm)	$4\pi M$ (G)	ℓ (μm)	$10^{-4} K_u$ (ergs/cm^3)	q
1/26/77	1	$(SmTm)_3(FaGa)_5O_{12}$	2.7	1.8	-	-	-	-
	2	"	2.7	1.8	-	-	-	-
	3	"	2.7	1.8	-	-	-	-
	4	"	2.8	1.8	-	-	-	-
	5	<111> G^3 polished substrate						
2/18/77	1	$(YSmLu)_3(FeGa)_5O_{12}$	2.0	1.5	-	-	-	-
	2	"	2.5	1.4	-	-	-	-
	3	"	3.0	1.4	-	-	-	-
3/24/77	1	$(YSmLu)_3(FeGa)_5O_{12}$	3.1	1.8	559	0.138	2.85	2.3
	2	"	3.1	1.5	555	0.098	3.67	3.0
	3	"	3.1	1.5	548	0.098	3.76	3.2
	4	"	3.9	2.1	626	0.150	5.34	3.4
	5	<111> G^3 polished substrate						
4/21/77	1	$(YEuTm)_3(FeGa)_5O_{12}$	2.9	1.5	-	-	-	-
		"	2.7	1.5	-	-	-	-
	3	"	3.0	1.5	-	-	-	-
	4	"	2.9	1.5	-	-	-	-
	5	<111> G^3 polished substrate						
5/18/77	1	$(YSmLu)_3(FeGa)_5O_{12}$	2.0	1.2	-	-	-	-
	2	"	2.1	1.25	-	-	-	-
	3	"	2.3	1.35	-	-	-	-
	4	"	2.0	1.3	-	-	-	-
6/30/77	1	$(YSmTm)_3(FeGa)_5O_{12}$	2.4	1.8	690	0.169	11.45	6.2
	2	" "	3.3	2.0	832	0.160	10.7	3.9
	3	"	4.3	1.7	759	0.096	4.5	2.0
	4	"	3.5	1.75	762	0.117	6.3	2.7
7/25/77	1	$(YS_mTm)_3(FeGa)_5O_{12}$	2.2	2.5	377	0.298	1.81	3.2
	2	$(YSm)_3(FeGa)_5O_{12}$	4.3	3.75	-	-	-	-
	3	$(YSmLu)_3(FeGa)_5O_{12}$	2.4	1.5	559	0.122	2.89	2.33
	4	"	4.3	1.8	569	0.102	3.15	2.44
	5	G^3 <111> polished substrate						

APPENDIX B

TABLE 3 - Cont'd

TABULATION OF MAGNETIC DATA FOR SUBSTRATES AND LPE FILMS DELIVERED TO CONTRACT MONITOR

DATE OF SHIPMENT to WPAFB	SAMPLE NUMBER	SAMPLE COMPOSITION	FILM THICKNESS (μm)	ZERO-FIELD STRIPE WIDTH (μm)	4πM (G)	ℓ (μm)	$10^{-4}K_u$ (ergs/cm^3)	q
7/20/76	1	$(LaEuTm)_3(FeGa)_5O_{12}$	2.7	1.9	526.	0.171	5.9	5.3
	2	"	1.9	1.8	591.	0.197	6.8	4.9
	3	"	2.2	1.8	516.	0.180	5.7	5.4
	4	"	1.8	1.9	650.	0.220	7.5	4.5
8/2/76	5	$(YLaTm)_3(FeGa)_5O_{12}$	1.8	1.2	688.	0.100	1.6	0.6
	6	" (implanted)	2.9	1.5	551.	0.104	1.4	0.9
	7	" (implanted)	4.0	1.9	488.	0.121	1.2	1.1
	8	"	1.5	1.0	590.	0.086	1.3	0.7
	9	G^3 SUBSTRATE						
8/27/76	1	$(LaEuTm)_3(FeGa)_5O_{12}$	2.1	2.0	489.	0.219	6.2	6.5
	2	"	2.3	2.0	504.	0.208	6.4	6.3
	3	"	1.6	2.0	559.	0.247	7.1	5.7
	4	G^3 SUBSTRATE						
	5	$(LaEuTm)_3(FeGa)_5O_{12}$	1.5	1.9	512.	0.236	7.5	7.2
	6,7,8	"	3.6	2.6	533.	0.239	6.6	5.8
9/29/76	1	$(YSmLuCa)_3(FeGa)_5O_{12}$	2.2	2.2	296.	0.248	0.97	2.8
	2	"	2.3	2.2	291.	0.241	0.87	2.6
	3	"	2.1	2.0	325.	0.219	0.89	2.1
	4	"	1.9	2.0	289.	0.231	0.75	2.2
	5	G^3 SUBSTRATE						
10/29/76	5-1	G^3 SUBSTRATE						
	5-2	$(LaEuTm)_3(FeGa)_5O_{12}$	1.6	1.9	563.	0.231	7.4	5.9
	5-3	$(EuTm)_3(FeGa)_5O_{12}$	2.0	2.3	-	-	-	-
	5-4	$(SmTm)_3(FeGa)_5O_{12}$	3.6	2.1	645.	0.161	12.2	7.4
	5-5	$(YSmLuCa)_3(FeGe)_5O_{12}$	1.7	2.0	376.	0.242	1.1	1.9
12/3/76	1	$(LaEuTm)_3(FeGa)_5O_{12}$	2.7	2.0	588.	0.186	6.8	4.9
	2	$(TbTm)_3(FeGa)_5O_{12}$	2.6	2.8	-	-	-	-
	3	"	3.1	2.5	-	-	-	-
	4	"	2.1	2.2	-	-	-	-
	5	G^3 SUBSTRATE						
12/15/76	1	$(TbTm)_3(FeGa)_5O_{12}$	1.9	1.4	-	-	-	-
	2	"	2.0	1.7	-	-	-	-
	3	"	1.6	1.9	-	-	-	-
	4	G_3 SUBSTRATE						

APPENDIX B

TABLE 3 - Cont'd

TABULATION OF MAGNETIC DATA FOR SUBSTRATES AND LPE FILMS DELIVERED TO CONTRACT MONITOR

DATE OF SHIPMENT to WPAFB	SAMPLE NUMBER	SAMPLE COMPOSITION	THICKNESS (μm)	STRIPE WIDTH (μm)	4πM (G)	ℓ (μm)	$10^{-4}K_u$ (ergs/cm^3)	q
8/30/77	1	$(YSmLu)_3(FeGa)_5O_{12}$	3.2	4.4	263	0.607	2.66	9.65
	2	"	5.2	3.0	480	0.229	7.06	7.7
	3	"	4.1	2.5	396	0.20	2.24	3.59
	4	$(YSm)_3(FeGa)_5O_{12}$	4.3	-	-	-	-	-
	5	<111> G^3 polished substrates						
10/4/77	1	$(SmTm)_3(FeGa)_5O_{12}$	2.4	1.8	699	0.169	0.114	6.16
	2	$(YSmTm)_3(FeGa)_5O_{12}$	1.5	1.45	-	-	-	-
	3	"	2.0	1.69	562	0.173	6.44	5.13

APPENDIX C

This is a preprint of a presentation to be given at the Conference on Magnetism and Magnetic Materials in Minneapolis November 8-11, 1977. The paper is entitled "$(YSmLu)_3(FeGa)_5O_{12}$ for 1 to 3 μm Diameter Bubble Devices," and is Abstract Number 1A-6 in the program booklet.

$(YSmLu)_3(FeGa)_5O_{12}$ FOR 1 TO 3 μm-DIAMETER BUBBLE DEVICES*

M. Kestigian, A. B. Smith and W. R. Bekebrede
Sperry Research Center, Sudbury, Massachusetts 01776

ABSTRACT

Investigations of small-bubble-diameter crystalline garnet LPE magnetic films have shown that $(YSmLu)_3(FeGa)_5O_{12}$ has some important advantages relative to other garnet compositions for use in bubble devices. In the present study, this material is compared with $(YSmLuCa)_3(FeGe)_5O_{12}$, a material widely used for device applications because of its desirable bubble properties. It is observed that in the gallium garnet, the growth process is much easier to control and is not subject to the inhomogeneities noted in the analogous calcium germanium composition. Furthermore, a detailed comparison of the properties of these two materials indicates that their small-bubble-diameter properties are very similar. These data include the Curie temperature and bubble-shift velocity, as well as the temperature dependence of stripe width, collapse field, anisotropy, magnetization and characteristic material length. The most noticeable difference revealed by these measurements is the expected lower Curie temperature of the gallium garnet; however, this has a relatively small effect on the temperature dependencies of stripe width and collapse field at device operating temperatures.

INTRODUCTION

The accepted and most promising method to obtain the low magnetic moments generally required for device operation involves the substitution of tetravalent germanium for iron, with an equal concentration of divalent calcium entering the dodecahedral site for charge compensation. Such compositions were reported first by Bonner et al [1] followed by other investigators [2 - 6]. These publications described the advantages of CaGe compositions for greater than 3 μm-diameter cylindrical-domain applications. These advantages are associated with the germanium cation residing almost entirely in the tetrahedral garnet sites, with very little germanium occupying the octahedral site [7]. This situation does not prevail if Ga or Al are used to obtain low $4\pi M$ values as, for example, in $(YSm)_3(FeGa)_5O_{12}$ [4]. Over 10% of these non-magnetic ions also substitute for the octahedral iron, thereby counteracting the tetrahedral iron dilution. Any such non-magnetic dilution of the octahedral iron sublattice will result in lowering the Curie temperature [8]. On the other hand, to obtain good temperature stability of magnetic properties, the Curie temperature of the garnet film must be kept as high as possible. For this reason, the CaGe-substituted rare earth iron garnets have been selected almost universally for 3-to 8-μm diameter bubble devices.

However, CaGe compositions have some disadvantages which should be considered. Inhomogeneities have been observed [9] in these materials if rigorous growth procedures are not adhered to. These inhomogeneities have not been a problem in the growth of Ga-garnet films, where the deposition process is much easier to control. Furthermore, as bubble diameters are lowered to approximately 2 μm, $4\pi M$ must be increased; therefore, smaller concentrations of the nonmagnetic cation diluent are required. The difference in Curie temperature between Ga- and CaGe-containing garnets then becomes sufficiently small [5] that one may question whether there is any practical difference for device use. This study was undertaken to answer that question by comparing $(YSmLu)_3(GaFe)_5O_{12}$ and $(YSmLuCa)_3(GeFe)_5O_{12}$.

EXPERIMENTAL TECHNIQUES

All of the garnet films reported herein were grown by the liquid-phase epitaxial dipping method [10]. Film deposition was carried out at a melt temperature of 980 to 1010° C, depending on the exact composition of the solution. Polished and cleaned <111>-oriented gadolinium gallium garnet (3G) substrates were used throughout this study. The substrates were held in a horizontal position during the dipping process. A rotation of 60 rpm with direction reversal every three seconds was used to obtain uniform magnetic film thickness. On withdrawal from the solution, the rotation was immediately accelerated to 600 rpm to remove any flux residue that might have adhered to the film. A growth rate of 0.5 to 1.0 μm/min was used in these experiments. A typical solution composition in terms of mole % is: Y_2O_3(0.457), Sm_2O_3(0.113), Lu_2O_3(0.18), Fe_2O_3(8.50), Ga_2O_3(0.79), PbO(84.77), B_2O_3(5.19). The magnetic films were grown lattice matched to 3G. Adjustments were made in the concentration ratios of the raw materials to maintain this condition.

The film magnetic parameters were determined using a polarizing microscope setup which was conventional except for the addition of a special television system (model 161A/142A; ITP Inc., Sunnyvale, Ca.) that aids greatly in making measurements on these small-bubble materials. Values of stripe width w, bubble collapse field H_{col}, magnetization $4\pi M$, characteristic length ℓ, anisotropy constant K_u, bubble stability factor q, Curie temperature T_c and mobility μ were obtained using standard techniques [11 - 16].

The samarium concentrations we have measured in these films are relative values only, obtained from x-ray spectroscopy measurements. No absorption or enhancement corrections were applied, but the samarium intensities were normalized by referring them to the iron intensities. The iron content of the films can be considered approximately constant as a result of selecting films having essentially the same magnetizations and thicknesses. Of course there will be a small octahedral site occupancy by gallium and lutetium which would require different iron contents for the same values of $4\pi M$, but we estimate this error would not exceed 5%.

RESULTS

In order to compare the temperature dependencies of $(YSmLu)_3(GaFe)_5O_{12}$ with its CaGe analog $(YSmLuCa)_3(GeFe)_5O_{12}$, we present data on two pairs of carefully selected films. In each pair, one film is a CaGe-garnet, while the other is a Ga-garnet; however, the room-temperature values of ℓ, $4\pi M$ and K_u are virtually the same for both films. In the first pair of films that we shall consider, both are approximately 2.5 μm-diameter-bubble materials†. The temperature dependencies of w, H_{col}, ℓ, $4\pi M$, H_k

†In order for the two films in each pair to have the same magnetic properties, we find that they must be formulated to have approximately the same Sm content. To maintain film/substrate lattice match, the CaGe-garnet must therefore contain more Lu (and less Y) than the Ga-garnet. In fact, to obtain the comparison in Fig. 1, it was necessary to formulate the Ga-garnet without any Lu. Except where otherwise noted, all the other films we shall discuss do contain Lu.

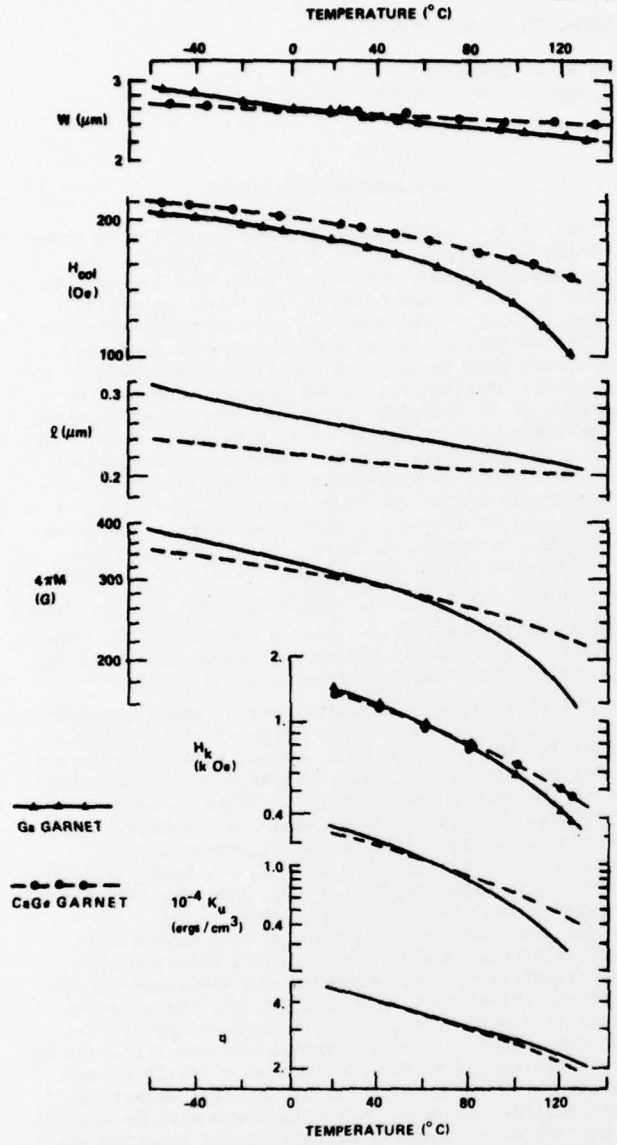

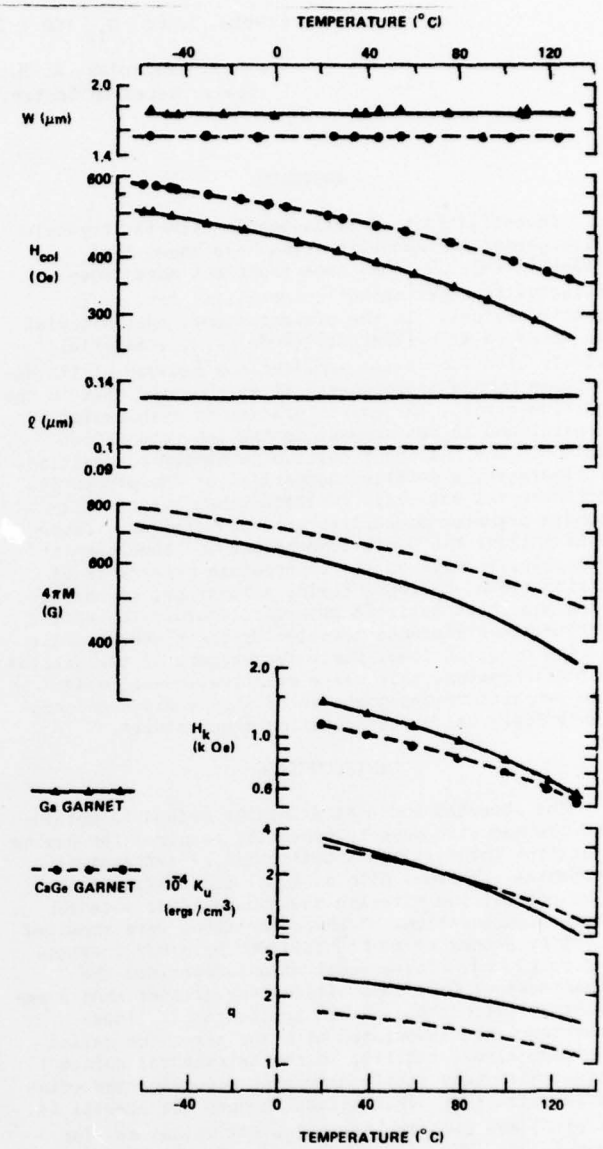

Figs. 1 and 2. A comparison of the temperature dependence of $(YSmLu)_3(GaFe)_5O_{12}$ and $(YSmLuCa)_3(GeFe)_5O_{12}$. (Thickness values for these particular films are: Fig. 1: 3.8 μm CaGe, 3.1 μm Ga; Fig. 2: 3.2 μm CaGe, 3.1 μm Ga.)

and q of these films are shown in Fig. 1. (Please note that logarithmic vertical coordinates have been used so that relative percentage changes can be easily visualized.) It will be seen from this figure that the temperature dependence of the Ga-garnet is more pronounced than that of the CaGe-garnet. However, this difference largely disappears when one considers materials such as those in Fig. 2 which support bubbles smaller than 2 μm in diameter. (It should be noted that the same vertical scales are used in Figs. 1 and 2 so that direct comparisons of temperature variations between these two figures can be made.)

The variation of Curie temperature with 4πM that we have measured in both the Ga- and CaGe-garnets is shown in Fig. 3. Even though T_c for the Ga-garnet is lower for all values of 4πM, the data in Fig. 2 demonstrate that when 4πM $\gtrsim$ 600 G, this difference does not appreciably affect bubble parameters below ~100° C.

The question naturally arises as to whether $(YSmLu)_3(GaFe)_5O_{12}$ garnets can be made to provide even smaller values of ℓ and/or higher q's than the material in Fig. 2. Since one would expect the anisotropy to increase with increasing Sm content and since film-substrate lattice match will require that the Y

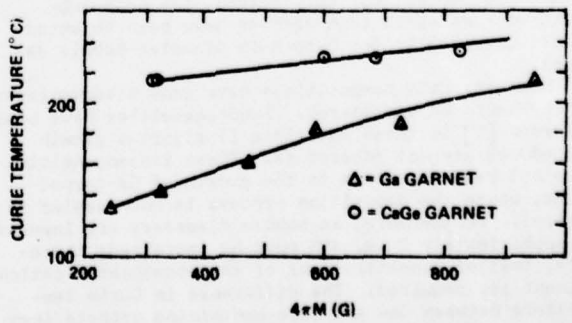

Fig. 3. Curie temperature for $(YSmLu)_3(GaFe)_5O_{12}$ and $(YSmLuCa)_3(GeFe)_5O_{12}$ films as a function of 4πM.

content be reduced in order to increase the Sm content, we have prepared a film with no Y [17,18] to see what anisotropy could be achieved. This film has a K_u of 8.8×10^4 ergs/cm^3 which is a factor of 2.7 higher than the Ga-containing film of Fig. 2. We should, therefore, be able to prepare films with an ℓ/q ratio which is $\sqrt{2.7} = 1.6$ times larger than that of the film in Fig. 2 (because the basic definitions of q and ℓ require that $q \propto \ell \sqrt{K}$). Thus, for example, a film could be made with the same q as the one in Fig. 2 but with ℓ being $1/1.6 = 60\%$ as large.

We have stated that we expect the anisotropy of $(YSmLu)_3(GaFe)_5O_{12}$ to depend on Sm content. It is clearly not a simple linear relationship, since the magnitude of the growth-induced anisotropy [19] can depend on other factors; and even if concentration were the only variable, the dependence is not linear. Nevertheless, it is interesting to plot K_u against Sm content as we have done in Fig. 4. As expected, $(YSm)_3(GaFe)_5O_{12}$ (which has the lowest Sm content) also has the lowest anisotropy, and $(LuSm)_3(GaFe)_5O_{12}$ (which has the highest Sm content) has the highest anisotropy. The other points show a roughly proportional relationship, although there are 3 points having the same Sm content but significantly different values of anisotropy.

The mobilities of each of the samples of Fig. 1 and 2 and the above-discussed $(SmLu)_3(FeGa)_5O_{12}$ are presented in Fig. 5. We have chosen to plot these mobilities against K_u to display the obvious correlation between these two parameters for films whose other properties are similar. (We are not attempting to deal with the fundamental questions [20] of the exact funtional dependence of mobility on K_u or other material parameters.) Figure 5 demonstrates that the Ga-garnet and CaGe-garnet exhibit similar trade-offs when one attempts to maximize both mobility and anisotropy, as is required for small-bubble device applications.

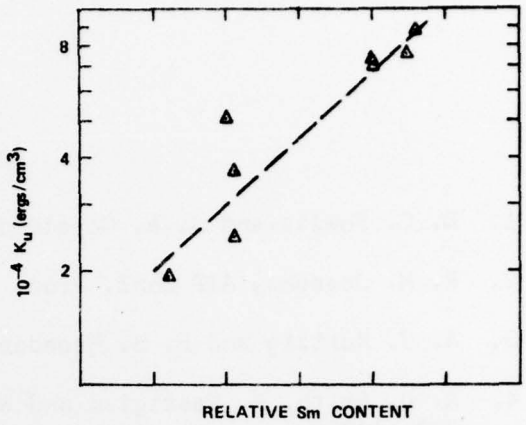

Fig. 4. Anisotropy constant K_u as a function of Sm content in a series of $(YSmLu)_3(GaFe)_5O_{12}$ garnet films. (The lowest anisotropy film shown here contains no Lu. The highest anisotropy film contains no Y. All other films contain Y, Sm, and Lu.)

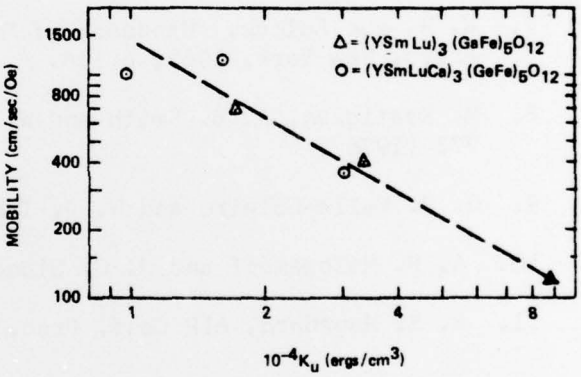

Fig. 5. Mobility vs K_u for $(YSmLu)_3(GaFe)_5O_{12}$ and $(YSmLuCa)_3(GeFe)_5O_{12}$ garnets. (Central four data points are for the samples of Figs. 1 and 2. The lowest mobility Ga-garnet in this figure contains no Y. The highest mobility Ga-garnet shown here contains no Lu. All other points represent samples containing Y, Sm and Lu.)

CONCLUSIONS

LPE films of $(SmLu)_3(GaFe)_5O_{12}$ and $(YSmLu)_3(GaFe)_5O_{12}$ have been grown and evaluated for 1- to 3-μm-bubble-diameter applications. A comparison of $(YSmLu)_3(GaFe)_5O_{12}$ with its calcium-germanium analog composition shows that the temperature dependencies of all the static bubble parameters are practically identical below 120 C if the material is formulated to have a bubble diameter < 2 μm. The mobilities are also similar for compositions which have approximately the same anisotropy constant.

REFERENCES

*Partially supported by WPAFB Contract No. F44620-76-C-0121.

1. W. A. Bonner, J. E. Geusic, D. H. Smith, L. G. van Uitert, and G. P. Vella-Coleiro, Mat. Res. Bull. 8, 1223 (1973).
2. W. A. Bonner, AIP Conf. Proc. 18, 68 (1974).
3. W. A. Bonner, Mat. Res. Bull. 10, 15 (1975).
4. J. W. Nielsen, S. L. Blank, D. H. Smith, G. P. Vella-Coleiro, F. B. Hagedorn, R. L. Barnes, and W. A. Biolsi, J. Elect. Mats. 3, 693 (1974).
5. J. E. Davies, E. A. Giess, and J. D. Kuptsis, J. Mat. Sci. 10, 589 (1975).
6. G. G. Sumner and W. R. Cox, AIP Conf. Proc. 34, 157 (1976).
7. S. Geller, H. J. Williams, G. P. Espinosa, and R. C. Sherwood, Bell Syst. Tech. J. 43, 565 (1964).
8. S. L. Blank, J. W. Nielsen and W. A. Biolsi, J. Elec. Soc. 123, 856 (1976).
9. M. Kestigian, A. B. Smith, and W. R. Bekebrede, Mat. Res. Bull. 11, 773 (1976).
10. H. J. Levinstein, R. W. Landorf, S. J. Licht and S. L. Blank, Appl. Phys. Letters 19, 486 (1971).
11. D. C. Fowlis and J. A. Copeland, AIP Conf. Proc. 5, 240 (1972).
12. A. J. Kurtzig and F. B. Hagedorn, IEEE Trans. MAG-7, 473 (1971); W. T. Stacy, M. M. Janssen, J. M. Robertson and M. J. G. van Hout, AIP Conf. Proc. 10, 314 (1972); A. B. Smith, M. Kestigian, and W. R. Bekebrede, AIP Conf. Proc. 10, 309 (1972).
13. W. F. Druyvesteyn, J. W. F. Dorleijn and R. J. Rijnierse, J. Appl. Phys. 44, 2397 (1973).
14. A. B. Smith, M. Kestigian, and W. R. Bekebrede, IEEE Trans. MAG-12, 579 (1976).
15. T. L. Hsu and D. W. Bellavance, IEEE Trans. MAG-8, 275 (1972).
16. G. P. Vella-Coleiro and W. J. Tabor, Appl. Phys. Lett. 21, 7 (1972).
17. J. T. Carlo, D. C. Bullock, R. E. Johnson and S. G. Parker, AIP Conf. Proc. 29, 105 (1975).
18. D. C. Bullock, J. T. Carlo, D. W. Mueller and T. L. Brewer, AIP Conf. Proc. 24, 647 (1974).
19. H. Callen, Mat. Res. Bull. 7, 931 (1971); A. Rosencwaig and W. J. Tabor, AIP Conf. Proc. 5, 57 (1971).
20. F. B. Hagedorn, AIP Conf. Proc. 5, 72 (1971).

REFERENCES

1. D. C. Fowlis and J. A. Copeland, AIP Conf. Proc. 5, 240 (1971).

2. R. M. Josephs, AIP Conf. Proc. 10, 286 (1972).

3. A. J. Kurtzig and F. B. Hagedorn, IEEE, Trans. MAG-7, 473 (1971).

4. A. B. Smith, M. Kestigian and W. R. Bekebrede, AIP Conf. Proc. 10, 309 (1972).

5. W. T. Stacy, M. M. Janssen, J. R. Robertson and M. J. G. vanHout, AIP Conf. Proc. 10, 314 (1972).

6. W. F. Druyvesteyn, J. W. F. Dorleijn and P. J. Rijnierse, J. Appl. Phys. 44, 2397 (1973).

7. W. H. Von Aulock, "Handbook of Microwave Ferrite Materials," Academic Press, New York, 1965, p 114.

8. M. Kestigian, A. B. Smith and W. R. Bekebrede, Mat. Res. Bull. 11, 773 (1976).

9. G. P. Vella-Coleiro and W. J. Tabor, Appl. Phys. Lett. 21, 7 (1972).

10. A. P. Malozemoff and J. C. Slonczewski, IEEE Trans. MAG-11, 1091 (1975).

11. F. B. Hagedorn, AIP Conf. Proc. 18, 222 (1973).